Stanford Exploration Project, Report 73, November 18, 1997, pages 1–22

Multi-component source equalization

Martin Karrenbach[1]

keywords: *acquisition, amplitudes, prestack, least squares, elastic, one-dimensional, deconvolution, wavelet*

ABSTRACT

Source equalization is necessary when source behavior changes with location within a given survey. Conventional robust methods characterize source differences as pure amplitude variations, assuming identical source time functions. I am extending this idea to vector wave fields, with the aim of preparing the data to be useful in elastic parameter determination (not just imaging). The method I have employed estimates source-location and source-component-consistent differences in the data. Those differences are parameterized as short 1-D filters in time and consequently correct the data to an average isotropic response. This is a meant to be a step toward the goal of determining absolute radiation patterns. Determining the exact radiation pattern is a more difficult task and requires an estimate of subsurface parameters, while the method shown here works without one having to know any medium properties. The source equalization solves a least squares problem in a way that is consistent in regard to source-location and source-component without trying to shape the wavelet as done in surface-consistent deconvolution. The least squares problem is solved in the time domain using the conjugate gradient method. Results from a 9-component land data set show that this procedure equalizes the data mostly by doing differential rotations and slight modifications of the source time function. The algorithm, although designed for multi-component data, is directly applicable to conventional single component data.

INTRODUCTION

In previous SEP reports I have proposed ways to remove effects of unequal radiation patterns in multi-component data. This subject is especially interesting in regard to diminishing biases introduced in inversion results and AVO, but even effects such as uneven stacks can be caused by unequal radiation patterns. I am working on equalizing radiation patterns within a given survey, in a component-consistent and source-location-consistent manner (Karrenbach and Muir, 1989; Karrenbach, 1991).

[1]**email:** not available

Such an equalization can be carried out in various ways. In this paper I am merely considering equalization to quasi-isotropic patterns by using no subsurface information whatsoever. This equalization technique has the advantage of being purely a preprocessing step. The method I am using dictates a reciprocal experimental geometry. The filtering technique is closely related to prediction error filtering, but should not be confused with surface consistent deconvolution (Levin, 1987). I am not trying to shape the wavelet to a desired form, although this step could be easily incorporated into the algorithm.

SYMMETRIZING THE WAVE FIELD

I am using the basic notion of symmetry in a wave field, or to be more precise the lack thereof. To expand that idea, let us look at a single slice through a prestack data volume. Let the data depend on the following variables:

$$\mathrm{D}(\mathbf{x_r}, \mathbf{x_s}, \omega) = \mathrm{S}(\mathbf{x_s}, \omega) * \mathrm{G}(\mathbf{x_r}, \mathbf{x_s}, \omega) * \mathrm{R}(\mathbf{x_s}, \omega) + \mathrm{N}(\mathbf{x_r}, \mathbf{x_s}, \omega), \tag{1}$$

where S describes the source behavior, R describes the receiver behavior, and G governs pure propagation effects through the medium. N is an additive noise term. In an ideal world N would be zero, as in Figure 1. G represents the Green's function of the medium. It can be shown that since the anisotropic elastic wave equation is linear and self-adjoint, the discrete representation of the continuous function D has to be symmetric. That is,

$$\mathrm{S\ G\ R}\ =\ (\mathrm{S\ G\ R})^{\mathrm{T}}\ =\ \mathrm{R^T\ G^T\ S^T}. \tag{2}$$

This equation defines a measure for the symmetry of a given data set. The symmetric part of data is defined as

$$\mathrm{SYM} = \frac{(\mathrm{S\ G\ R}\ +\ \mathrm{R^T\ G^T\ S^T})}{2} \tag{3}$$

and the antisymmetric part of the data as

$$\mathrm{DEV} = \frac{(\mathrm{S\ G\ R}\ -\ \mathrm{R^T\ G^T\ S^T})}{2}. \tag{4}$$

Wave field types

Equation (2) can be used for acoustic wave fields or elastic wave fields with any degree of anisotropy. In the acoustic case, all elements in the discrete representation are just scalar values (pressure field). For the elastic case all scalars are replaced by three vectors. Using three vectors in R, means that we use three component receivers; if we also use three component receivers, we must use three vectors in S. Consequently, the

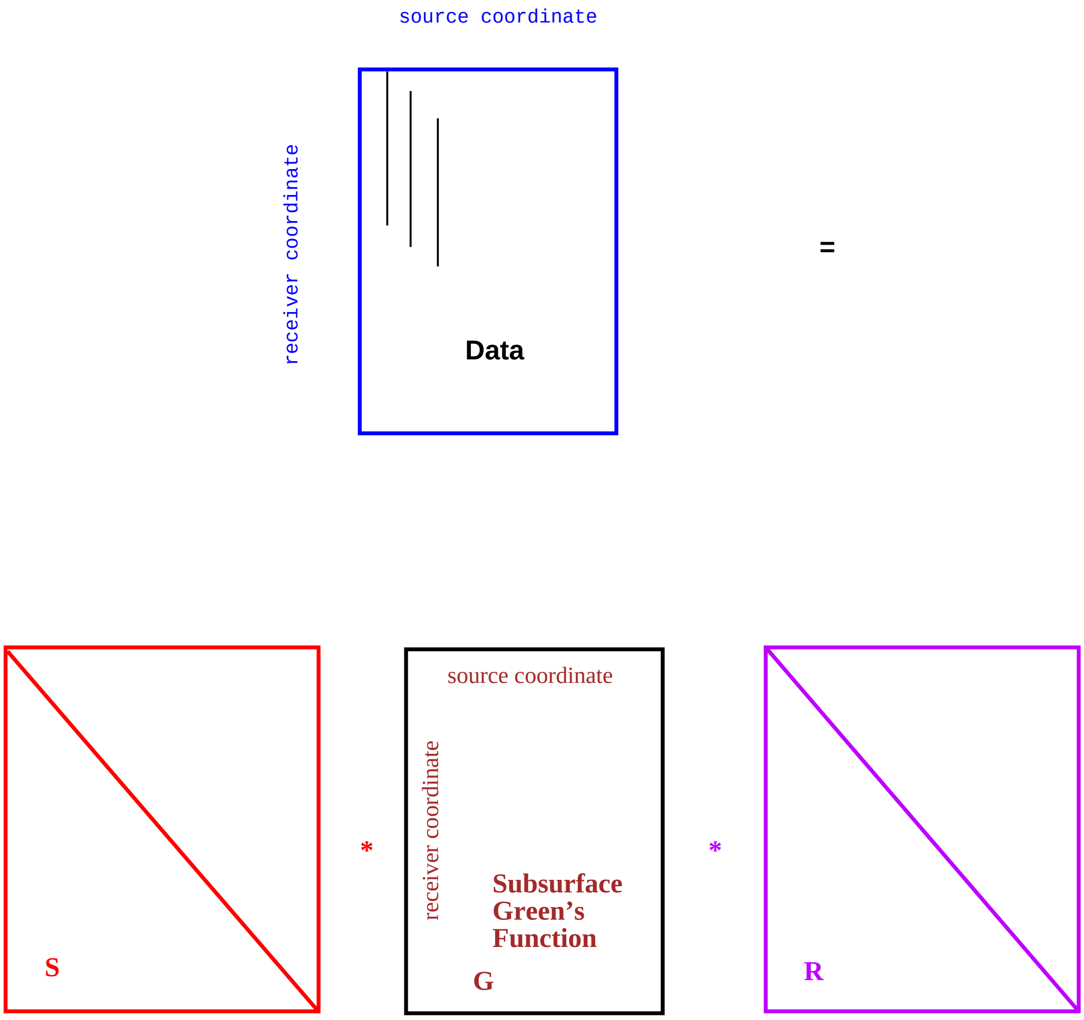

Figure 1: Schematic representation of a discrete symmetric wave field
martin2-matrix [NR]

elements in G are replaced by three-by-three block matrices. If we limit the number of components or employ wave type receivers or wave type sources, then mixtures of scalars and vectors appear in equation (2), but the analysis and the algorithm is still the same. The basic premise is still that we have a reciprocal acquisition geometry. Therefore this source equalization scheme is applicable to conventional single component data as well as multi-component data.

Symmetric data acquisition

The premise of reciprocal acquisition geometry is intimately related to symmetric data acquisition. The idea of symmetric wave field sampling was described by Ongkiehong (1988) and Vermeer (1991). Their recommendation is to record seismic data as generally as possible and perform data reduction later, in the processing step. Array forming is thus done not in the field but on the computer. This method, of course, requires sufficient dynamic range of recording equipment, but does not discriminate against propagation effects. Data are most unbiased if they are collected symmetrically, that is, for each (vector) source throughout the survey we must have a (vector) receiver at the same location. Ongkiehong and Vermeer show asymmetric sampling examples and their effects on stack arrays. The effect can be seen on the changes in amplitude changes with offset during migration and inversion. The acquisition geometry issue is independent of the type of experiment carried out and applies to scalar, as well as vector field, experiments. Symmetric sampling is a general notion and offers general guidelines for processing. Their conclusion is that symmetric acquisition geometry offers the best unbiased acquisition and allows the most flexibility in later preprocessing. I'd like to extend their observation and claim that reciprocal acquisition geometry offers the best unbiased acquisition and allows new directions in processing that data.

Figure 3 and 4 are examples of nearly reciprocal data acquisition. Figure 2 plots the source and receiver positions of a prestack multi-component data set. Besides one source gap, the acquisition geometry is regular. Each source is located between a receiver position. Figure 5 and 6 represent the symmetric and antisymmetric components of a time slice through the prestack data set. Source and geophone positions were interpolated by nearest neighbours before determining the amount of symmetry and deviation. The surprising result is that the symmetric part and the symmetric part are about the same magnitude. One would not expect this, if one thought that equation (2) holds for this data set. The lack of symmetry (or reciprocity) demands some explanation. I chose to explain it by differences in source behavior, assuming that differences in receiver behavior are small compared to the potentially nonlinear behavior of seismic sources. The lack of symmetry can be employed to set up a minimization problem, where the objective function maximizes symmetry in a source-location and source-component consistent way.

Figure 2: Pembrook 9-c data acquisition geometry is shown in source and receiver coordinates. This space is identical for all components. The recording is very regular, and nearly reciprocal. The source coordinates are between receiver coordinates. martin2-sgplot [ER]

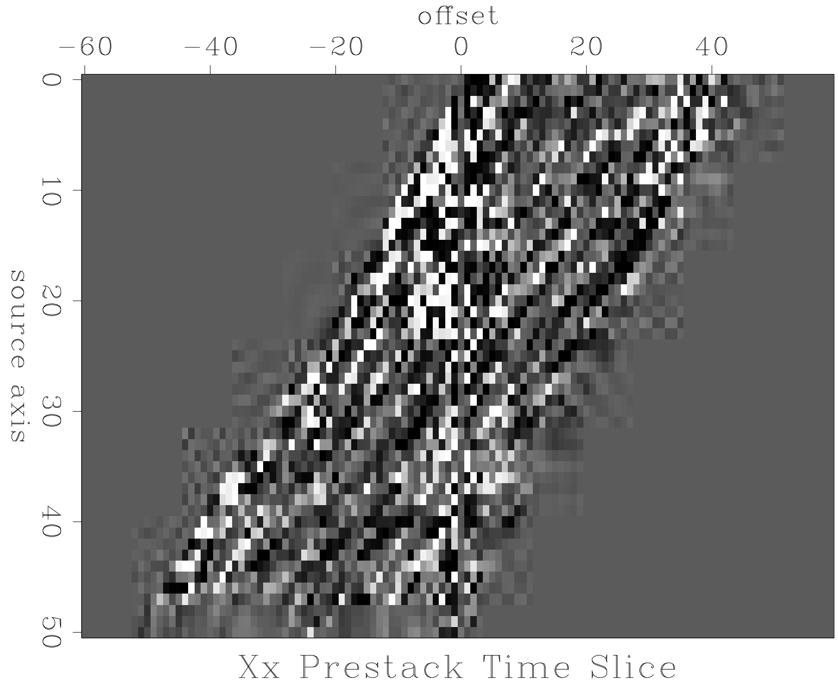

Figure 3: Time slices of the part of the data for which reciprocal data exist for 50 source points (Xx-component). To go through time slices, press the button. martin2-slicexx1 [ER]

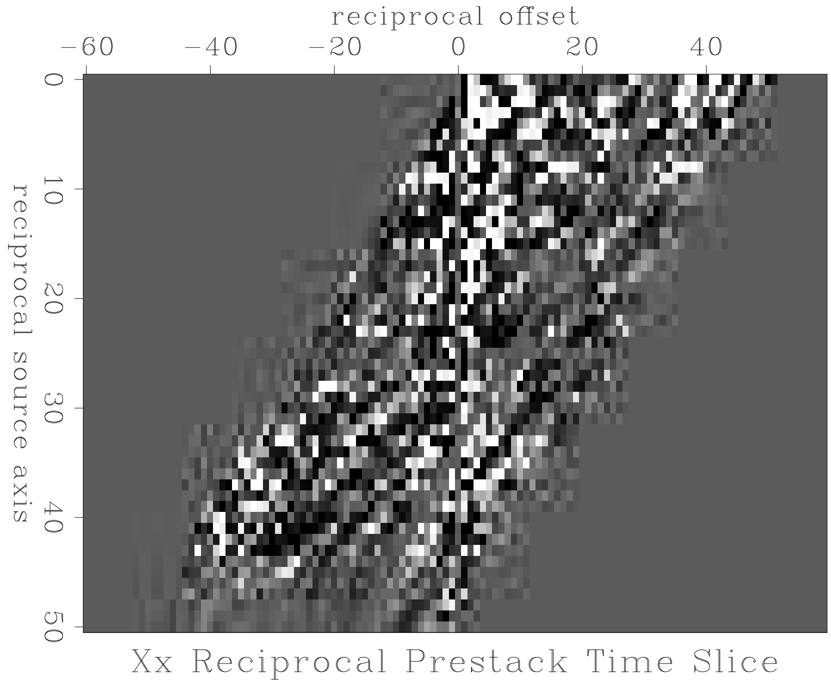

Figure 4: Reciprocal time slices of the part of the data for which reciprocal data exist for 50 source points (Xx component). To go through time slices, press the button. martin2-slicexx2 [ER]

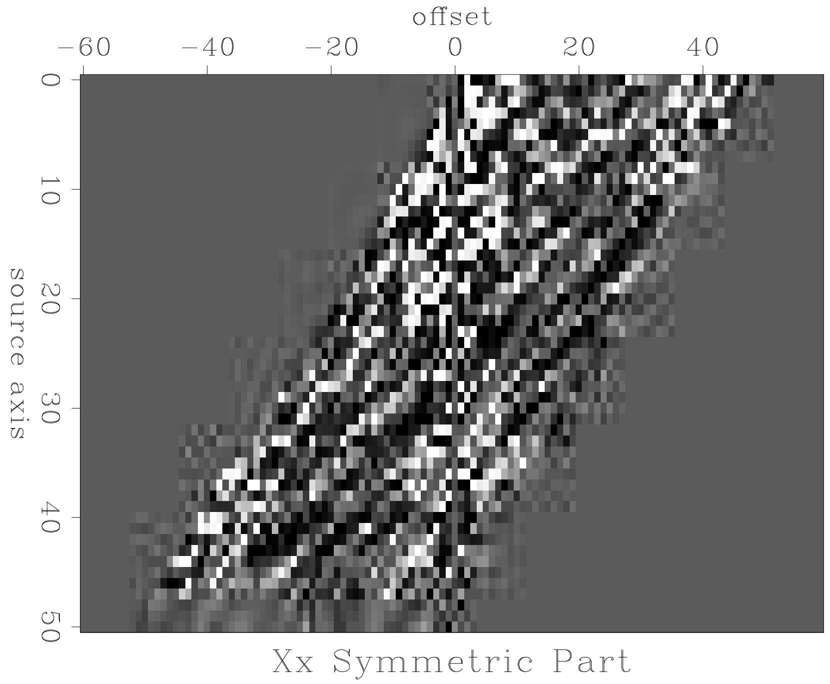

Figure 5: Symmetric part of the data (Xx-component). To go through time slices press the button. martin2-symslicexx [ER]

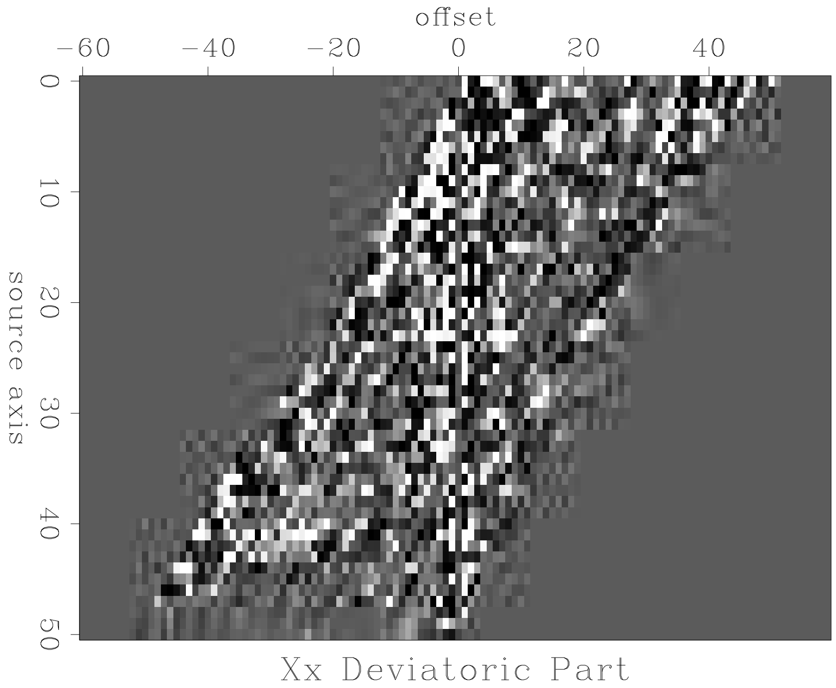

Figure 6: Antisymmetric part of the data (Xx-component). To go through time slices, press the button. martin2-devslicexx [ER]

THE OPTIMIZATION PROBLEM

I have set up a least-squares optimization problem in which I minimize the difference between data and its reciprocal counterpart. Analyzing the solution of that problem shows that none of the eigenvectors has a pure DC component. Thus the absolute radiation pattern cannot be determined. However, relative changes are perfectly resolvable within a cable length. This relativity requires us to specify a reference with respect to which the prediction error filters are computed. There are a multitude of choices. One possibility would be to average the sources over some range and establish the average as a reference source. The disadvantage of this method is that a relatively noisy (bad) common source gather biases the estimation procedure unfavourably. Another choice would be to design or give some training data as reference, but that would have the effect of wavelet shaping. Instead, I took the first source as a reference source, all other filters show differences with respect to that source. My initial guess is a single spike at the zero lag filter location. In the minimization process the filters are not constrained at all (except for being specified as to the number of filter coefficients). Once I decided on the filter shape (1-D, short), I tested the following objective functions governing the minimization process.

First, we find the global minimum of the squared difference for all the components at the same time. This requires simultaneous accessibility of all 9 component data. For each iteration that data must be read once.

$$E_1 = \sum_{i,j,k,l} \{ d_{ji}^{lk} * s_j^{lk} - d_{ij}^{kl} * s_i^{kl} \}^2. \tag{5}$$

E_1 represents the complete misfit of filtered data samples; i stands for the source and j are reciprocal source coordinates. The indices i and j trace all different source and reciprocal source locations. The indices l and k (source and reciprocal source components) both stay within the range $1, 2, 3$. The values of i and j may describe source location in 2-D or 3-D. Convolution is denoted by $*$. For each source location, the general shape of s^{kl} in E_1 is

$$\begin{pmatrix} s_{11}(t) & s_{12}(t) & s_{13}(t) \\ s_{21}(t) & s_{22}(t) & s_{23}(t) \\ s_{31}(t) & s_{32}(t) & s_{33}(t) \end{pmatrix}.$$

For pressure data, the index range for l and k degenerates to just being unity. For vector wave field data these indices indicate the type of component (vertical, horizontal, inline, crossline). To each ensemble a filter pair s_i^{kl} and s_j^{lk} is applied. In equation (5) s is estimated, for each source component pair, as a short function in time.

Instead of equalizing all components simultaneously, we can treat each reciprocal component pair separately. The advantage is smaller data sets to be worked on. Equation (6) gives the appropriate objective function. The filter s^{kl} is then a single scalar value for each separate minimization process. E_2^{kl} represents the objective function to be minimized.

$$E_2^{kl} = \sum_{i,j} \{ d_{ji}^{lk} * s_j^{lk} - d_{ij}^{kl} * s_i^{kl} \}^2 \tag{6}$$

A third minimization alternative, however, is to find a global minimum for a filter that consists of a scalar array multiplied by a source location filter, as follows

$$E_3 = \sum_{i,j,k,l} \{ d_{ji}^{lk} * (s_j^{lk} f_j^l) - d_{ij}^{kl} * (s_i^{kl} f_i^k) \}^2 \tag{7}$$

$$s_i^{lk} f_i^l = \begin{pmatrix} f_1(t) & 0 & 0 \\ 0 & f_2(t) & 0 \\ 0 & 0 & f_3(t) \end{pmatrix} \begin{pmatrix} s_{11} & s_{12} & s_{13} \\ s_{21} & s_{22} & s_{23} \\ s_{31} & s_{32} & s_{33} \end{pmatrix}$$

This filter decomposition honors the fact that for a single experiment with a given source orientation, the vector source function is separable and consistent in time for all source components. Such a filter compensates for mispositioning of the source vector by a rotation and for differences in the time history.

The Pembrook data set

The data set I am using is part of a 9-c surface seismic survey. The multi-component ARIS source was fired multiple times at a single source location. The data were then added and subtracted, to get vertical and horizontal inline and crossline components. These were the data conditions I used as input into the source equalization procedure, no other preprocessing was done. The data set satisfies the requirements described in the general outline of the source equalization process. The acquisition geometry is nearly reciprocal and quite regular.

RESULTS

The optimization problems described by E_1 and E_2 were solved using a conjugate gradient method. I chose to constrain the first filter in each of the series of filters to unity. Thus I chose the first shot gather to be my reference gather. Figure 7 and 8 show results obtained during testing the nonstationarity of the recorded data on a few shot gathers. I tried different window sizes and shapes, but the answers, after about 40 iterations, were always very similar to 7 and 8. This behavior encouraged me to apply the equalization process about 50 shotgathers in a two second time window, knowing that this time window averages over a fair amount of energy that is radiated from the source with different emergence angles. I chose to use a medium length filter of about 40 points (160 msec). Results of those equalizations are shown in two groups. First a minimization described by E_2 for the components Xx, Yy and Zz (capital letters denote source components, lower-case letters denote receiver components). The prediction error filters obtained are shown in Figures 9, 10 and 11. The filter obtained after about 40 iterations is minimum phase. There seem to be hardly any time shifts between different source points. The amplitude in the main peak and lower energy wavelet characterize all the filters consistently. Figure 12 shows a comparison between the raw prestack time slice and the filtered version. The differences in that time slice are small but noticeable. The continuity in character of the time slice is increased. Figures 13 to 21 are obtained from maximizing symmetry in the prestack data using the objective function E_1, where all components are equalized simultaneously. The offdiagonal elements in the three-by-three filter set show identical behavior. Again the filter are consistent along the line and exhibit the similar properties as the filters in Figures 9 to 11. The short 1-D filters equalize by averaging over an angular distribution of radiation pattern. The amount of averaging is determined by the time window and number of different arrivals within the time window.

In the future I plan to investigate how strong the influence of such an equalization is on the results produced by a simple stack, velocity analysis and migration, thus determining when it is necessary to estimate the radiation pattern in an absolute manner instead of, as shown here, a purely relative manner.

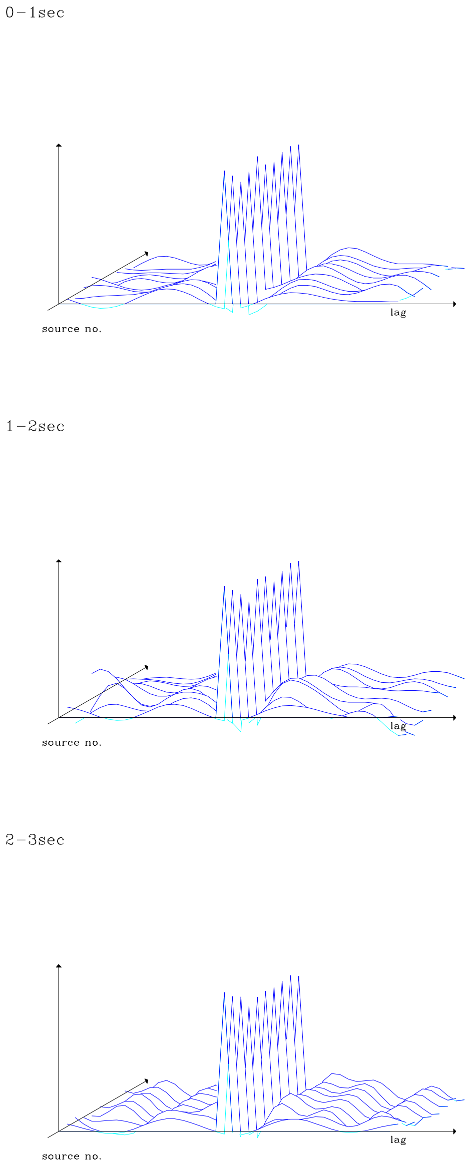

Figure 7: Prediction error filters at 10 locations estimated from 0-3 seconds in one-second-long windows of the data. $\boxed{\text{martin2-fig1}}$ [ER]

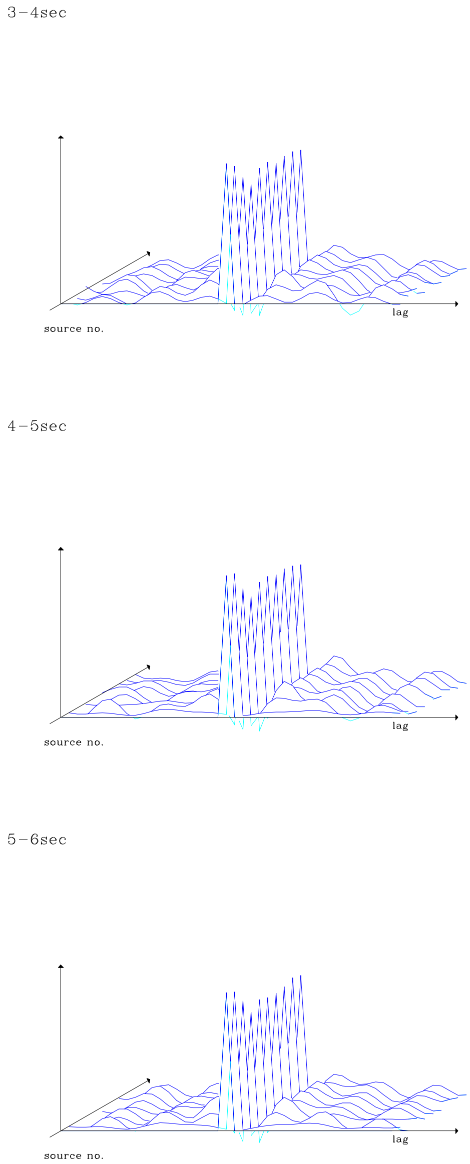

Figure 8: Prediction error filters at 10 locations estimated from 3-7 seconds in one-second-long windows of the data. martin2-fig2 [ER]

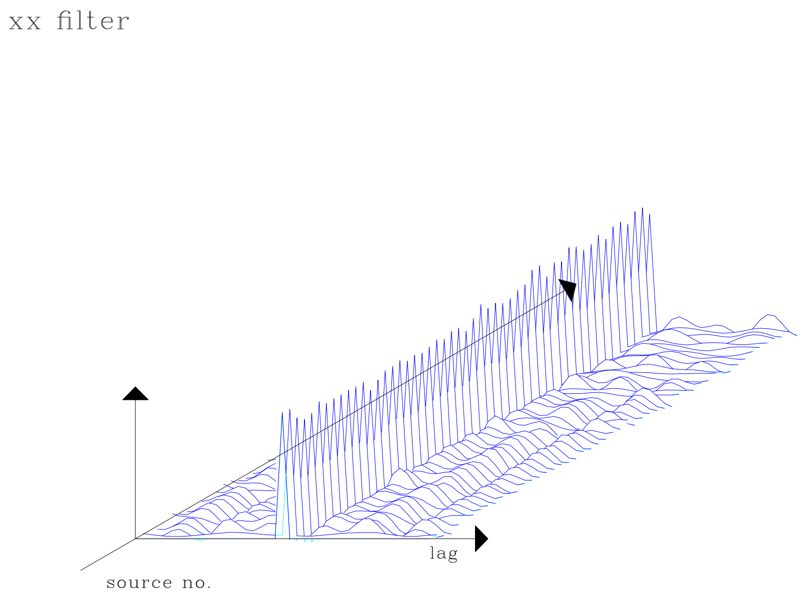

Figure 9: Prediction error filters at 50 locations estimated for X source component and x receiver component in a two-second-time window. Minimizes objective function E_2. martin2-filsxx [ER]

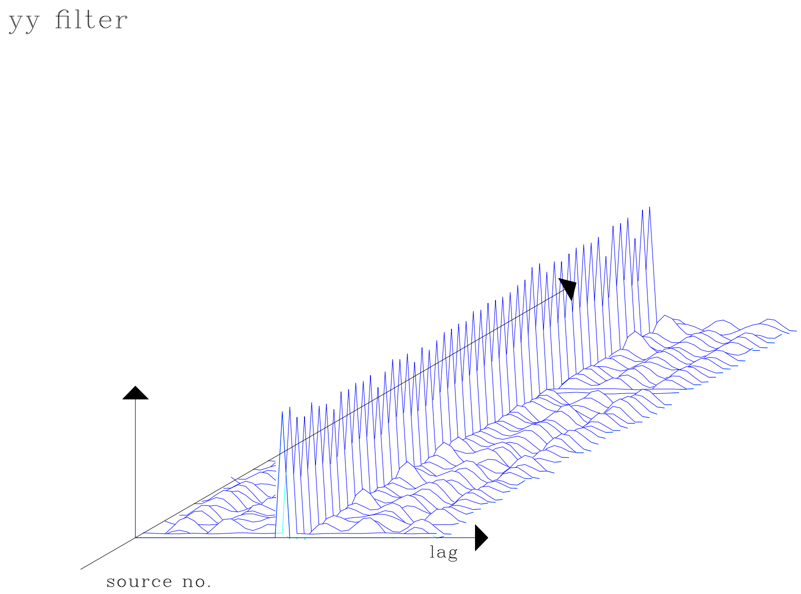

Figure 10: Prediction error filters at 50 locations estimated for Y source component and y receiver component in a two-second-time window. Minimizes objective function E_2. martin2-filsyy [ER]

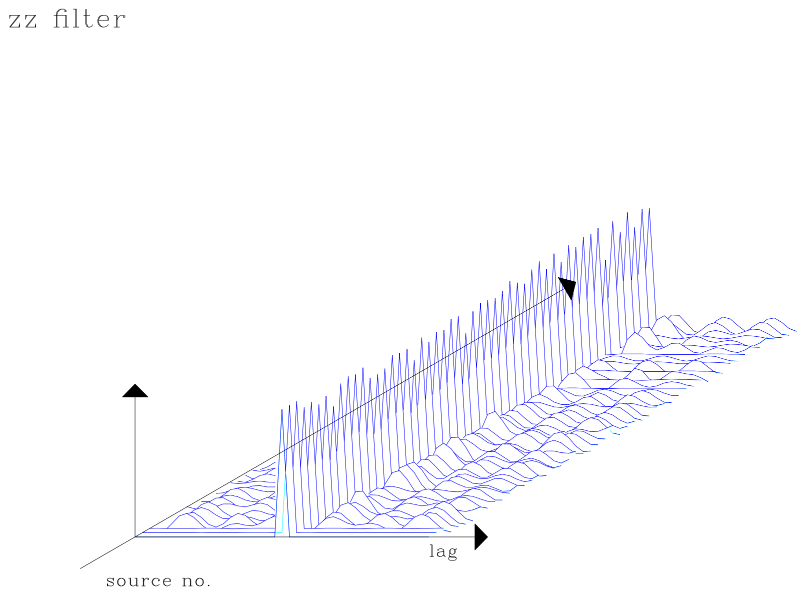

Figure 11: Prediction error filters at 50 locations estimated for Z source component and z receiver component in a two-second-time window. Minimizes objective function E_2. martin2-filszz [ER]

CONCLUSIONS

Multi-component source equalization can be carried out in the time domain using short 1-D filters. Reciprocal experimental geometry is necessary for this method to work properly. In the data example above data acquisition is nearly reciprocal and receiver locations can easily be interpolated onto source locations. No subsurface information such as velocity, density, or stiffness is necessary for performing the equalization. That makes this method a preferred preprocessing step. The disadvantages are the potentially low signal-to-noise ratio and the implicit averaging over source emergence angles. The estimated filters mainly show amplitude variations and small modifications to the source-time function. My next step is to check the influence of this equalization on data rotation, stacks, and migrated images. I plan to implement a similar scheme that estimates absolute radiation patterns with an approximate knowledge of subsurface properties.

ACKNOWLEDGMENTS

Chevron Oil Field Research Co. made this project possible by releasing the data and results. I am also indebted to Ray Ergas, Don Winterstein, Mark Meadows, and Clint Frasier for interesting discussions and for the opportunity of having a very exciting summer job. Finally I thanks Dave Nichols for his great team spirit and for his advice and discussions in the Lab, as well as at the beach. Thanks to David Lumley for his careful proofreading and suggestions.

REFERENCES

Karrenbach, M., and Muir, F., 1989, Turning multi component data into tensor fields: SEP–**60**, 235–242.

Karrenbach, M., 1991, Moving source and receiver position by slant stacks: SEP–**72**, 65–72.

Levin, S., 1987, Deconvolution with spatial constraints: Ph.D. thesis, Stanford University.

Ongkiehong, L., and Askin, H. J., 1988, Towards the universal seismic acquisition technique: The Leading Edge, **6**, no. 2, 46–63.

Vermeer, G. J. O., 1991, Symmetric sampling: The Leading Edge, **10**, no. 11, 21–27.

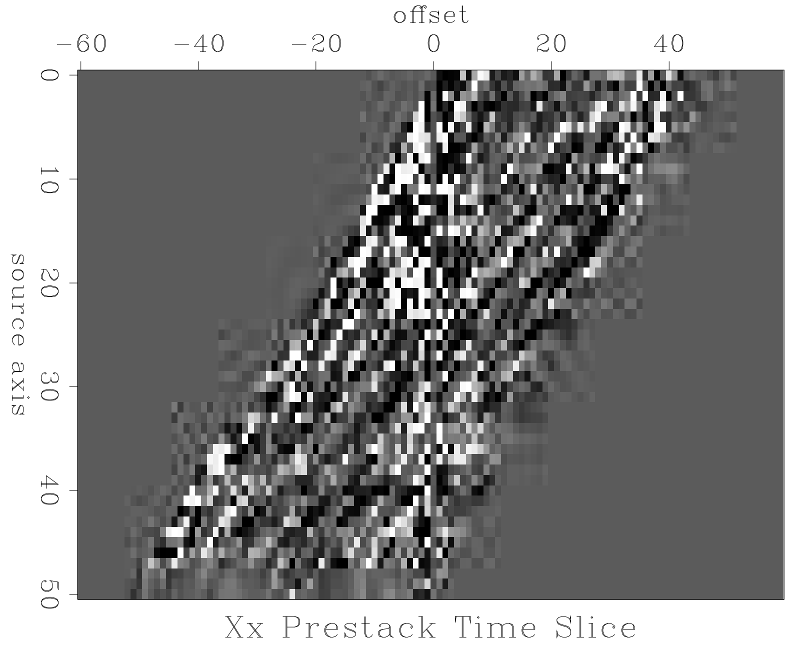

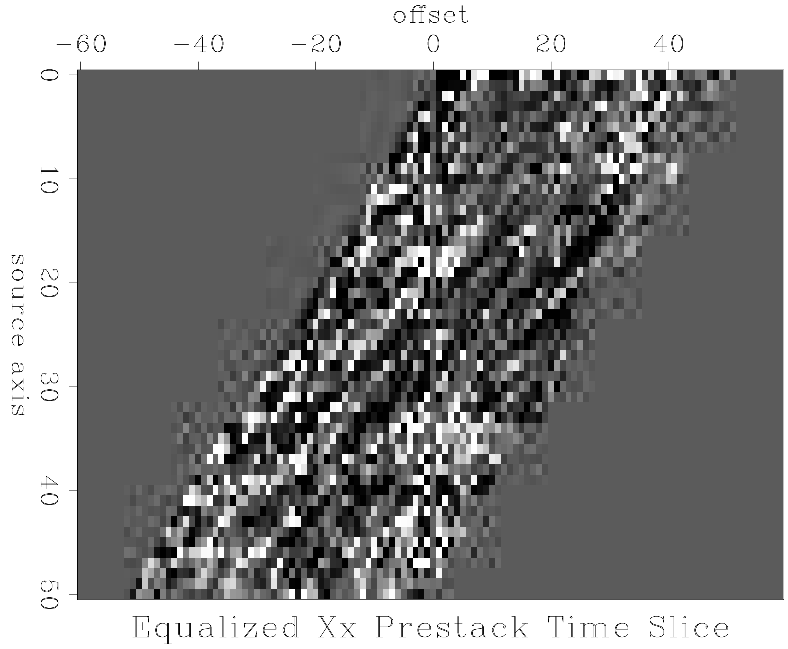

Figure 12: Raw and equalized time slice of the part of the data for which reciprocal data exist for 50 source points (Xx-component). To go through time slices, press the button. martin2-compxx [ER]

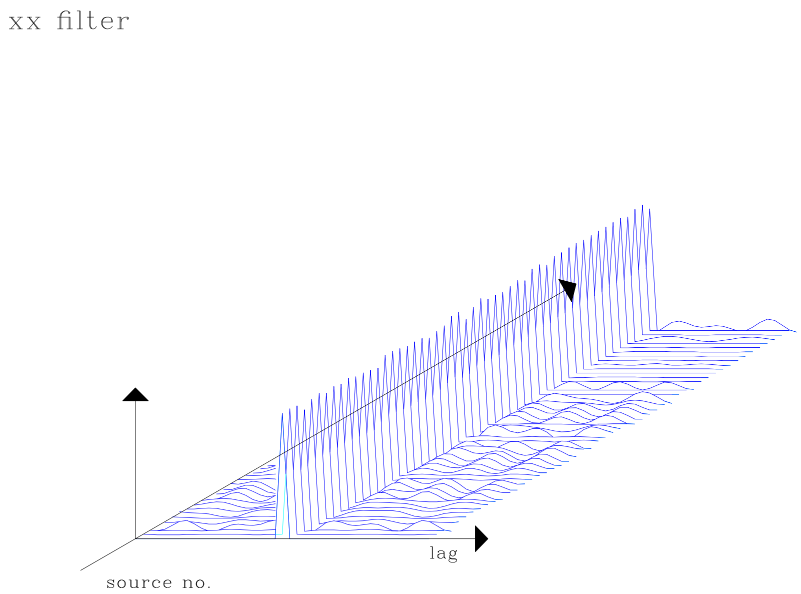

Figure 13: Prediction error filters at 50 locations estimated for X source component and x receiver component in a two-second-time window. Minimizes objective function E_1. martin2-filxx.40 [ER]

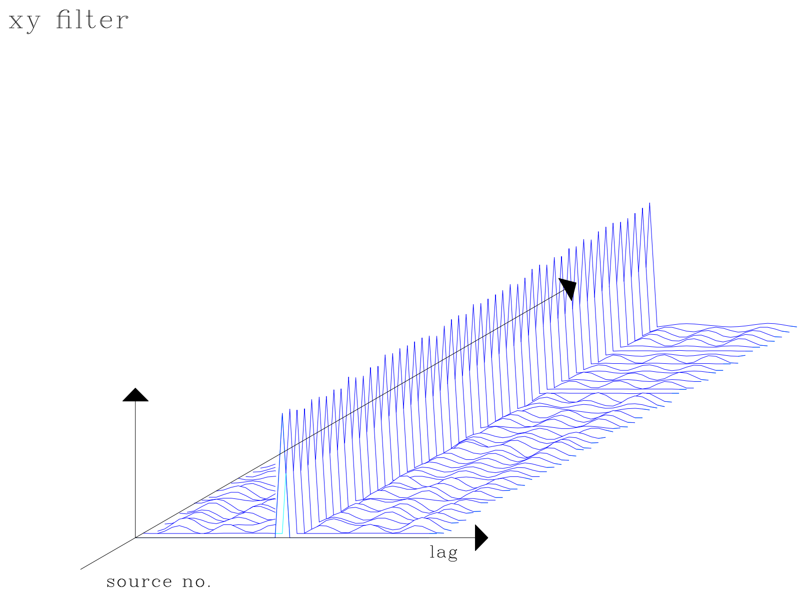

Figure 14: Prediction error filters at 50 locations estimated for X source component and y receiver component in a two-second-time window. Minimizes objective function E_1. martin2-filxy.40 [ER]

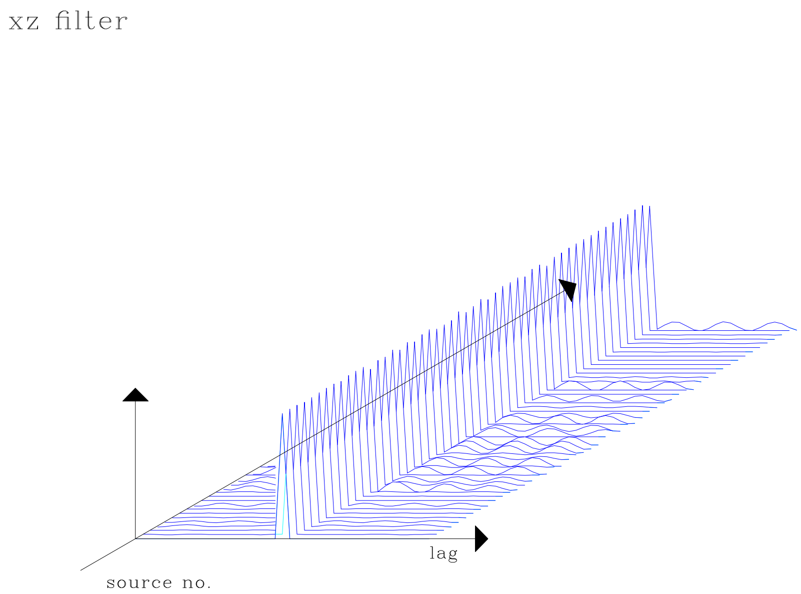

Figure 15: Prediction error filters at 50 locations estimated for X source component and z receiver component in a two-second-time window. Minimizes objective function E_1. martin2-filxz.40 [ER]

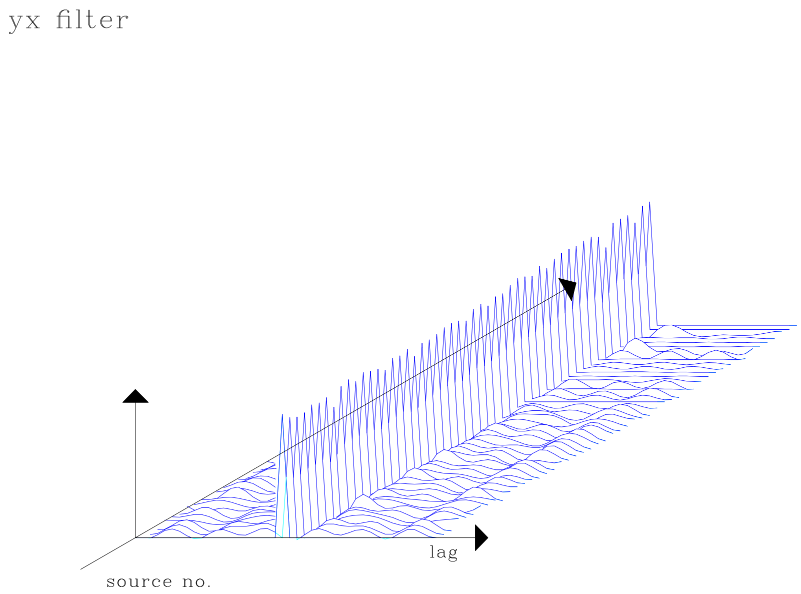

Figure 16: Prediction error filters at 50 locations estimated for Y source component and x receiver component in a two-second-time window. Minimizes objective function E_1. martin2-filyx.40 [ER]

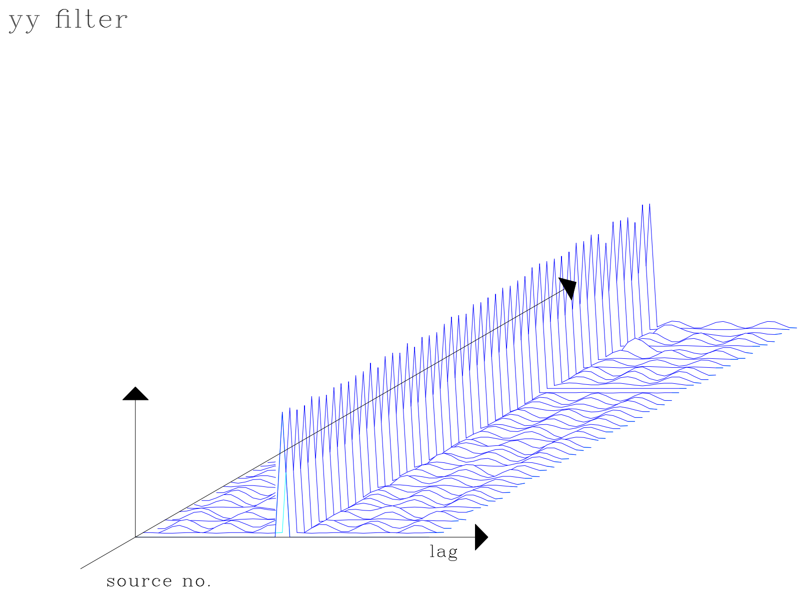

Figure 17: Prediction error filters at 50 locations estimated for Y source component and y receiver component in a two-second-time window. Minimizes objective function E_1. martin2-filyy.40 [ER]

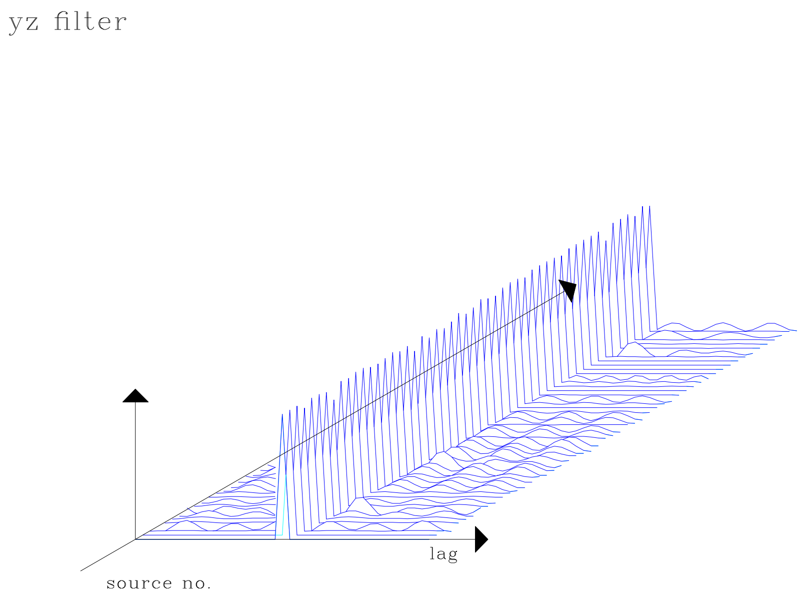

Figure 18: Prediction error filters at 50 locations estimated for Y source component and z receiver component in a two-second-time window. Minimizes objective function E_1. martin2-filyz.40 [ER]

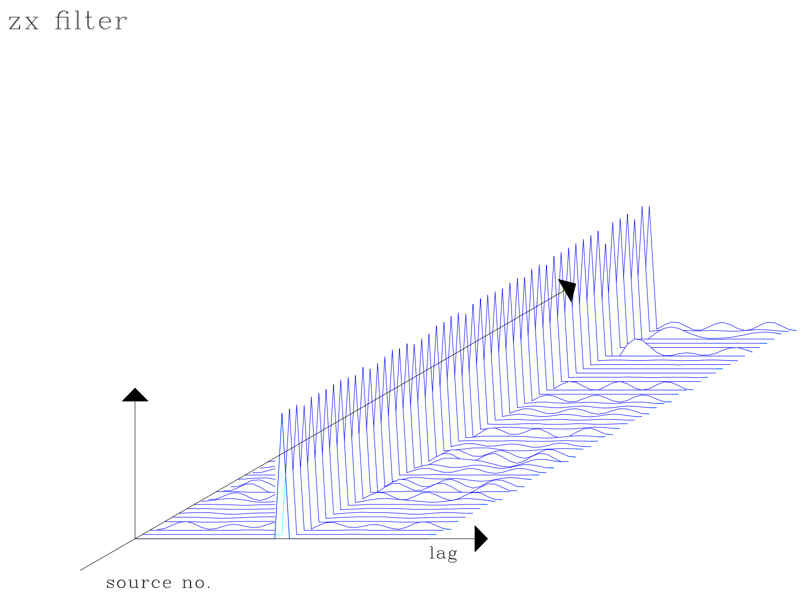

Figure 19: Prediction error filters at 50 locations estimated for Z source component and x receiver component in a two-second-time window. Minimizes objective function E_1. martin2-filzx.40 [ER]

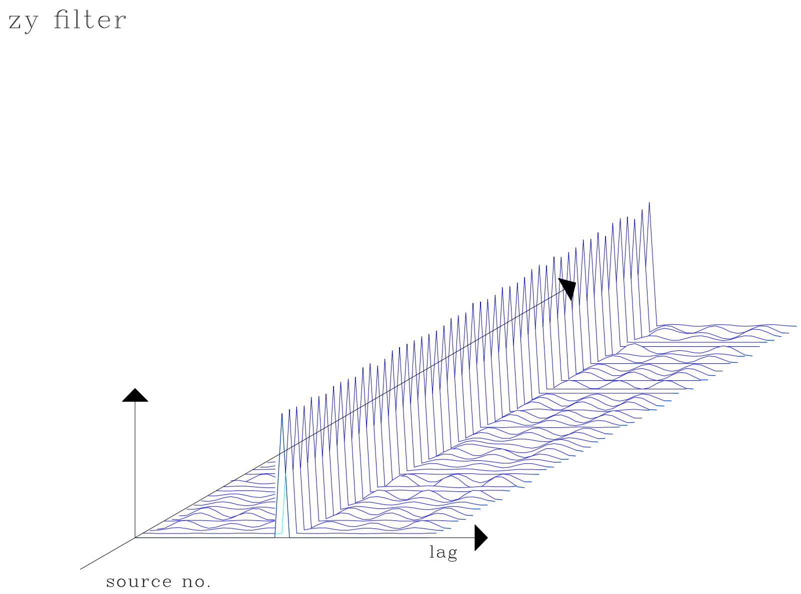

Figure 20: Prediction error filters at 50 locations estimated for Z source component and y receiver component in a two-second-time window. Minimizes objective function E_1. martin2-filzy.40 [ER]

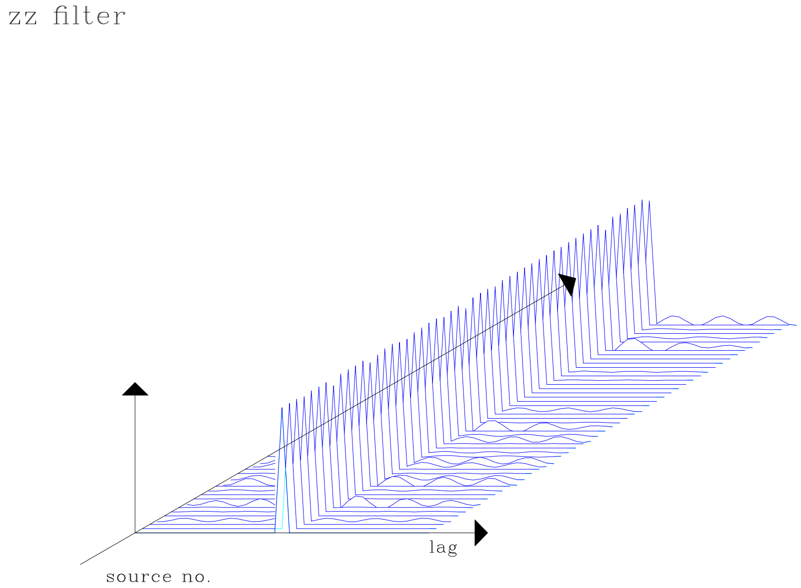

Figure 21: Prediction error filters at 50 locations estimated for Z source component and z receiver component in a two-second-time window. Minimizes objective function E_1. martin2-filzz.40 [ER]